Journal of Integrative Neuroscience, Vol. 5, No. 2 (2006) 199–222

Imperial College Press
www.icpress.co.uk

Research Report

DIRECT CONTROL OF FIRING RATE GAIN BY DENDRITIC SHUNTING INHIBITION

CHARLES CAPADAY*

Brain & Movement Laboratory, Department of Anatomy and Physiology
Laval University, CRULRG F6500
2601 de la Canardiere Québec City G1J 2G3, Canada
charles.capaday@anm.ulaval.edu

CARL VAN VREESWIJK

Neurophysique et Physiologie du système moteur
CNRS UMR 8119, 45 rue des Saints Pères, 75270, Paris, France
carl.van-vreeswijk@biomedicale.univ-paris5.fr

Received 3 October 2005
Revised 17 November 2005

The firing rate gain of neurons, defined as the slope of the relation between input to a neuron and its firing rate, has received considerable attention in the past few years. This has been largely motivated by the many experimental demonstrations of behavior related gain changes in a variety of neural circuits of the CNS. A surprising result was that a prime candidate, shunting inhibition, apparently does not change the firing rate gain of neurons. However, in this paper, we show a physiologically plausible mechanism by which shunting inhibition in the dendritic tree does, in a simple and direct manner, modulate the firing gain of neurons. The effect is due to a strong attenuation of the dendritic current arriving at the soma by shunting dendritic inhibition. Increasing the dendritic inhibitory conductance enhances the attenuation of current flowing from the dendritic to the somatic compartment and thus reduces firing gain. This mechanism relies on known physiological and anatomical properties of CNS neurons and does not require special features such as tunable neural noise inputs. Gain control by the proposed mechanism may prove to be a ubiquitous feature of neural circuit operations and it is readily verifiable experimentally.

Keywords: Multiplication; gain modulation; membrane conductance; firing gain; motoneurons.

1. Introduction

A large number of experimental studies in a variety of neural systems have demonstrated that the firing rate gain of neurons can change during behavior. For example,

*Corresponding author.

the gain through the first sensory relay nucleus of weakly electric fish is modified without a significant change of the baseline spontaneous activity of the output E-cells of this nucleus [5, 6]. Similarly, the H-reflex is reduced in the stance phase of human walking, in comparison to voluntary activation at matched levels of motor activity (reviewed in Ref. 12). In area 7a of monkey parietal cortex, a neuron's response to visual inputs depends in a multiplicative way on the position of the eye in the orbit [3]. Such experimental observations have spurred on studies to elucidate the mechanisms by which the firing rate gain of neurons may be controlled [12, 13, 15, 16, 24, 32, 38]. The focus of this work has been at the level of the single neuron, notwithstanding that the experimental data was obtained from neural systems with complex network topologies that can inherently produce gain changes.

It is now well established that mixtures of postsynaptic excitatory and inhibitory inputs into the soma have little, if any, effect on firing rate gain [12, 13, 24, 30]. Based on a single numerical study of a complicated model neuron, Holt and Koch concluded that dendritic shunting inhibition also does not change the firing rate gain. In response to these results, several groups have investigated more elaborate single cell mechanisms for gain control [15, 32, 36].

These mechanisms have in common that they rely on stochastic membrane potential fluctuations, referred to as noise, to effect a change in gain. There is disagreement on the nature of gain control by membrane noise. Chance *et al.* [15] proposed that excitatory and inhibitory inputs acting in the background control gain, whilst added excitatory inputs produce firing. This gain control mechanism assumes excitatory and inhibitory inputs be balanced so as not to affect the resting membrane potential. It is not clear how this balance, or other noise parameters, may be controlled by neural circuits. Mitchell and Silver [32] proposed that gain control may be achieved in a simpler way with tonic background inhibition and noisy excitatory inputs. Yet another mechanism was proposed by Prescott and De Koninck [36], who suggested that noise itself has a relatively small influence on firing gain, but coupled to a process termed dendritic saturation, gain modulation is considerably enhanced for inputs on dendrites.

One remarkable feature of the model studied in [36] is its similarity to the original work by Holt and Koch [24], which indicated that in a very similar model inhibitory inputs, arriving at the dendrite does *not* lead to a change in gain. Therefore, we have a situation in which two numerical studies suggest opposite results for dendritic shunting inhibition. What is needed to disambiguate the situation is an understanding of the possible mechanism that may lead to a change in gain through dendritic shunting inhibition. Here, we present a simple two compartment (2-C) integrate and fire (IF) model in which this issue can be studied analytically, and the mechanism can be understood. We also perform simulations of a conductance based 2-C model to show that the mechanism does not rely on special features of the IF model.

2. Models

The focus of the mathematical analysis and numerical simulations presented herein is on 2-C models. We begin with an integrate-and-fire 2-C model following the parallel resistor-capacitor neuron model first proposed by Lapicque [25]. The integrate-and-fire (IF) model allows the derivation of analytical expressions that relate the current threshold required for firing to the conductances activated at the somatic and dendritic compartments. From this, the relation between firing rate and activated conductances follows. The expression readily explains how firing gain may be modulated. A conductance based α-motoneuron model is then used to demonstrate that the analytical results derived for the IF model are applicable for a generic repetitively firing neuron model. The numerical outputs of the α-motoneuron model are directly comparable to the experimental data.

2.1. *Analytically tractable model*

We construct a two compartment integrate and fire (IF) neuron, for which the firing rate can be determined analytically. To describe such a model, we first reconsider the standard IF neuron [25], and then use this to formulate a 2-C model with a soma that acts as an IF neuron attached, by a coupling conductance, to a passive dendritic compartment.

2.1.1. *Single compartment IF neuron*

In the IF neuron the voltage, V, relative to the resting potential, satisfies

$$C\frac{dV}{dt} = -g_l(V - V_l) + I_0(t), \tag{2.1}$$

where C is the membrane capacitance, g_l the leak conductance, V_l is the leak reversal potential which we will assume to be 0, and I_0 the current injected into the cell. When the voltage reaches its threshold value, V_{T}, the neuron spikes and voltage is reset to the reset potential, V_{r}. Alternatively, we may write

$$C\frac{dV}{dt} = -g_l V + I_0(t) + I_{\mathrm{spike}}(t), \tag{2.2}$$

where I_{spike} is the current that induces the spike and resets the voltage.

In a single compartment, the action potential itself is usually neglected, and only the reset after the spike is taken into account. However, in a conductance-based model neuron that has a somatic and a dendritic compartment, the spike in the soma will have the effect of depolarizing the voltage in the dendrite. Thus, the spike cannot be neglected. Spikes are characterized by large voltage excursions of short duration. Their effect on the dendrite is proportional to the product of the height and width of the spike. We can mimic this in the IF neuron by taking the limit where the spike duration is infinitely short, while keeping the area under the

spike constant. Thus, if the spikes occur at times $t = t_k$, the voltage of the neuron is given by the voltage of Eq. (2.1) or (2.2), to which a term $\sum S\delta(t - t_k)$ is added. S is the area under the spike, while $\delta(t)$ is the Dirac delta function. S has the dimension voltage $\times$ time. The spike can be incorporated in the current I_{spike} by writing I_{spike} as

$$I_{\text{spike}}(t) = \sum_k SC\delta'(t - t_k) + [Sg_l - C(V_{\text{T}} - V_{\text{r}})]\delta(t - t_k). \tag{2.3}$$

Here $\delta'(t)$ is the derivative of the delta function, $\delta'(t) = d\delta(t)/dt$. Using this, one can integrate Eq. (2.2) to obtain the evolution of the voltage including the spike. Note that the spike times t_k have to be consistent with the voltage trace; the voltage at time t_k has to satisfy $V(t_k) = V_{\text{T}}$.

2.1.2. *A two-compartment IF neuron*

We can generalize this to an IF neuron with more than one compartment. We consider a two-compartment model that consists of a soma that acts as an IF neuron, which is coupled to passive dendritic compartment. The current from the soma to the dendrite is equal to $g_C(V_S - V_D)$. g_C is the conductance between the compartments, V_S is the somatic voltage and V_D the dendritic voltage. The voltage of the dendrite satisfies

$$C_D\frac{V_D}{dt} = -g_D V_D + I_D(t) + g_C(V_S - V_D), \tag{2.4}$$

where C_D is the capacitance of the dendritic compartment, g_D is its membrane conductance, and $I_D(t)$ is the current injected into the dendritic compartment.

The voltage of the soma obeys

$$C_S\frac{V_S}{dt} = -g_S V_S + I_S(t) + I_{\text{spike}}(t) + g_C(V_D - V_S), \tag{2.5}$$

where C_S, g_S and $I_S(t)$ are the soma's capacitance, membrane conductance and input current respectively. Using $I_{\text{spike}}(t)$ as defined by Eq. (2.3) leads to an ambiguity, since the spike current depends on the membrane conductance, and it is not immediately clear which conductance to take. One could take the conductance g_S, or $g_S + g_C$, or something in between. If V_D would follow V_S extremely closely, so that the term $g_C(V_D - V_S)$ were negligible, the right choice would likely be g_S. On the other hand, if V_D was independent of V_S, one should take $g_S + g_C$. The reality is somewhere between these extremes, and we will use an effective conductance, g_{eff}, that takes this into account. To determine g_{eff}, we calculate the steady state voltage V_{SS} of the soma when a constant sub-threshold current I_S is applied to the soma and the effective conductance as the ratio between the latter and the former, $g_{\text{eff}} = I_S/V_S S$.

With a sub-threshold current, the neuron does not spike, so we can determine the steady state voltage using Eqs. (2.4) and (2.5) with $I_{\text{spike}} = 0$. Thus, we obtain for the effective conductance

$$g_{\text{eff}} = g_S + g_C \frac{g_D}{g_D + g_C}. \tag{2.6}$$

To recapitulate, in the two-compartment IF neuron, the dendritic voltage obeys Eq. (2.4) and the somatic voltage Eq. (2.5), in which I_{spike} is given by

$$I_{\text{spike}}(t) = \sum_k SC_S\delta'(t - t_k) + [Sg_{\text{eff}} - C_S(V_{\text{T}} - V_{\text{r}})]\delta(t - t_k), \tag{2.7}$$

with g_{eff} given by Eq. (2.6). In this description, the effect of the spike can also be described in the following way: If the cell fires an action potential at time t_k, the somatic voltage is immediately reset from V_{T} to $V_{\text{r}} - g_C^2 S/[C_S(g_D + g_C)]$, while the dendritic voltage is increased by an amount $g_C S/C_D$.

$$V_S(t^-) = V_{\text{T}} \Rightarrow \begin{cases} V_S(t^+) \to V_{\text{r}} - \frac{g_C^2}{g_D+g_C}\frac{S}{C_S} \\ V_D(t^+) \to V_D(t^-) + g_C\frac{S}{C_D} \end{cases}. \tag{2.8}$$

It should be noted that in this description, the voltage of the soma is *not* reset to V_{r}, but to a lower value instead. This is to compensate for the fact that dendritic voltage is increased during the spike. As the two compartments are coupled, this increase in the dendritic voltage leads to an extra current into the somatic compartment, for which the lower reset compensates.

To better understand this mechanism, it is useful to consider the case where g_C is very large. In this limit, one would assume that the neuron could be treated as an effective single compartment cell. Yet, the reset voltage, $V_{\text{reset}} = V_{\text{r}} - g_C^2 S/[C_S(g_D + g_C)]$ becomes very negative, while on the other hand, the dendritic voltage just after the spike $V_D(t^+) = V_D(t^-) + g_C S/C_D$ will reach a very large positive value. However, one can show that on a timescale $\tau = g_C(C_D + C_S)/C_D C_S$, which is much shorter than the soma's and dendrite's membrane time constants, both voltages evolve to the same value, $V_S \approx V_D \approx (C_D V_D(t^-) + C_S V_{\text{r}})/(C_D + C_S)$. Therefore, except for immediately after the spike, the two voltages are indeed almost identical and the neuron can be treated as a single compartment cell. The somatic and dendritic voltage are very different during and just after the spike, due to our description of the spike as an event with zero duration. If we have chosen a description of the spike with a finite duration, the two voltages would also be the same during the spike.

2.1.3. *Synaptic currents*

So far, we have described the model's response to the current injected in the somatic or dendritic compartment. Inputs mediated through synapses have two effects. They inject currents into the cell and increase the effective membrane conductance. For

a dendritic compartment with a leak conductance g_{lD}, that receives synaptic input with conductances g_{eD} and g_{iD} for the excitatory and inhibitory synapses respectively, V_D satisfies

$$C_D\frac{dV_D}{dt} = -g_{lD}V_D - g_{eD}(V_D - V_e) - g_{iD}(V_D - V_i) + g_C(V_S - V_D), \tag{2.9}$$

where V_e and V_i are the reversal potentials, relative to the threshold, of the excitatory and inhibitory synaptic currents. For a somatic compartment with a leak conductance g_{lS} and synaptic conductances g_{eS} and g_{iS}, V_S obeys

$$C_S\frac{dV_S}{dt} = -g_{lS}V_S - g_{eS}(V_S - V_e) - g_{iS}(V_S - V_i) + g_C(V_D - V_S) + I_{\text{spike}}. \tag{2.10}$$

This reduces to the model described above, if we set $g_S = g_{lS} + g_{eS} + g_{iS}$, $g_D = g_{lD} + g_{eD} + g_{iD}$ and write for the currents $I_S = g_{eS}V_e + g_{IS}V_I$ and $I_D = g_{eD}V_e + g_{iD}V_i$. Clearly, we can also account for cases in which synaptic inputs and injected currents are combined by setting $I_S = g_{eS}V_e + g_{IS}V_I + I_{0S}$, where I_{0S} is the applied current into the soma, and treat an applied input into the dendrite in a similar manner.

2.2. *Conductance based α-motoneuron model*

The basic physiological properties of spinal α-motoneurons and the parameter space needed to produce a model of this neuron are well characterized (e.g., Refs. 19, 22, 34 and 35). Thus, a simple α-motoneuron model was used as an example of a generic repetitively firing neuron [12, 13]. The purpose was not to produce a state-of-the-art model of α-motoneurons, but simply to use a physiologically plausible yet computationally tractable neuron model sufficient to explore the issues at hand (e.g., see Refs. 12 and 28). The results presented herein are derived from a 2-C model based on time and voltage dependent ionic conductances [12]. The model includes a dendritic compartment electrically coupled to an active somatic compartment.

2.2.1. *Computational procedures*

The motoneuron model used in the present simulations is described in detail in Capaday [12]. The values of the somatic conductances and time constants were taken from the extensive simulations of cat α-motoneurons done by Powers [34]; they are presented along with other simulation parameters in Table 1. The dendritic compartment was electrically coupled to the soma such that the ratio of dendritic to somatic conductance was ten. The effects of changing the coupling conductance on firing rate gain are also considered. The model includes resting (leak) somatic (g_{lS}) and dendritic conductances (g_{lD}) and excitatory (g_{eS}, g_{eD}) and inhibitory (g_{iS}, g_{iD}) conductances. The somatic and dendritic excitatory and inhibitory conductances were independently controlled. The resting membrane potential (V_r) was set to zero. When the spike threshold is reached — fixed at 10 mV more depolarized than V_r — the membrane potential is set to 90 mV for 1 ms, thus simulating the

Table 1. Parameter values used for the numerical simulation of the α-motoneuron model.

Parameters	Value(s)
Membrane Capacitances, C_S, C_D	0.55, 5.46 nF
Resting Conductances, g_{lS}, g_{lD}	0.1, 0.45 μS
Coupling Conductance, g_C	0.45 μS
Threshold and Resting Potential, V_{T}, V_{r}	10, 0 mV
Excitatory Reversal Potential, V_e	50 mV
Inhibitory and Potassium Reversal Potential, V_i, V_K	-10, -15 mV
Fast Potassium Conductance, G_{Kf}	0.7 μS
After Hyperpolarization Conductance, G_{ahp}	2.8 μS
Decay Time Constant, τ_{Kf}, of g_{Kf}	3 ms
Decay Time Constant, τ_{ahp}, of g_{ahp}	22 ms

occurrence of a spike [34]. The time of occurrence of spikes is explicitly determined in the simulations, from which the firing rate is calculated. Following the occurrence of a spike, a fast Potassium conductance (g_{Kf}) at the soma quickly repolarizes the motoneuron [4], whereas the slower Calcium-dependent after-hyperpolarization (AHP) conductance (g_{ahp}) regulates the firing rate [19, 29, 30]. The following pair of coupled differential equations gives the rate of change of membrane potential in each compartment

$$\begin{aligned} C_D\frac{dV_D}{dt} &= -g_{lD}V_D - g_{eD}(V_D - V_e) - g_{iD}(V_D - V_i) + g_C(V_S - V_D) \\ C_S\frac{dV_S}{dt} &= -g_{lS}V_S - g_{eS}(V_S - V_e) - g_{iS}(V_S - V_i) + g_{Kf}(V_K - V_S) \\ &\quad + g_{ahp}(V_K - V_S) + g_C(V_D - V_S), \end{aligned} \tag{2.11}$$

where V_K is the potassium reversal potential. Immediately after the first spike, the conductance for the fast potassium (g_{Kf}) and afterhyperpolarization (g_{ahp}) rapidly increase to the values G_{Kf} and G_{ahp} respectively. Between spikes, these conductances decay back to zero with time constants τ_{Kf} and τ_{ahp}. These conductances are saturating and their increase after subsequent spikes is decreased by an amount proportional to g_{Kf} and g_{ahp} respectively. For more details see Refs. 12 and 30.

This coupled pair of equations is non-linear and has no known analytical solution. Therefore, the time dependence of the membrane potential was obtained by numerical integration of the equation with respect to time. These simulations were performed in Mathcad, using a fourth-order Runge–Kuta integration scheme. The non-linearity is due to the product of the time-dependent AHP conductance with the membrane potential and more generally, any of the conductances that may be of non-linear functions of time or membrane potential. Further details on this model and analytical expressions to calculate the steady-state dendritic and somatic potentials and the attenuation of currents flowing from one compartment to the other are presented in Ref. 12.

3. Results

The results are divided in three sections. In the first two sections, the relations between firing rate and constant injected currents, or conductance changes, are derived for the IF model. From these equations, the mechanism by which gain modulation may be effected is readily apparent. Numerical simulation results based on these equations are then presented graphically to demonstrate the nature of the gain modulation. Details on the derivation of the equations are given in the appendix. In the third section, numerical simulation results, motivated by the derived analytical expressions, are presented for the α-motoneuron model. The purpose is to show that the analytical results derived from the IF model are applicable to more realistic conductance based neural models.

3.1. *Response of the IF neuron to constant inputs*

If the inputs I_S into the soma and I_D into the dendrite are constant, the neuron will fire periodically after a transient. To determine the firing rate, we make the Ansatz so that the voltages vary periodically with period T and determine T self-consistently.

Assuming that the neuron spikes at times $t_k = kT$, then just after the spike at time $t = 0$, the somatic voltage is given by $V_S(0^+) = V_\mathrm{r} - \frac{g_C^2 S}{C_S(g_D+g_C)}$; while just before the next spike at time $t = T$, the voltage is at the threshold, $V_S(T^-) = V_\mathrm{T}$. The voltage of the dendrite is augmented by an amount $g_C S/C_D$, and since the voltage of the neuron is periodic, with a period T, we have $V_D(0^+) = V_D(T^-) + g_C S/C_D$. In Appendix A, we show that this allows us to calculate the relation between the inputs, I_S and I_D, and the period. The input-output relation is given by

$$\begin{aligned}
&\tau_s(\lambda_+ - \lambda_-)\frac{V_S' + \tilde{g}_D V_D'}{1 - \tilde{g}_S\tilde{g}_D} \\
&\quad = \tilde{g}_S\tilde{g}_D S\left(\frac{\lambda_+ e^{-\lambda_+ T}}{1 - e^{-\lambda_+ T}} - \frac{\lambda_- e^{-\lambda_- T}}{1 - e^{-\lambda_- T}}\right) + V_\mathrm{T}\left(\frac{1 - \tau_S\lambda_-}{1 - e^{-\lambda_+ T}} - \frac{1 - \tau_S\lambda_+}{1 - e^{-\lambda_- T}}\right) \\
&\qquad + V_\mathrm{r}\left(\frac{(1 - \tau_S\lambda_+)^{-\lambda_- T}}{1 - e^{-\lambda_- T}} - \frac{(1 - \tau_S\lambda_-)e^{-\lambda_+ T}}{1 - e^{-\lambda_+ T}}\right),
\end{aligned} \tag{3.1}$$

where we have used $V_A' = I_A/(g_C + g_A)$, for $A = S$ or D, $\tilde{g}_S = g_C/(g_D + g_C)$ and $\tilde{g}_D = g_C/(g_S + g_D)$, while the parameters λ_+ and λ_- are given by

$$\lambda_\pm = \frac{1}{2\tau_S\tau_D}\left(\tau_S + \tau_D \pm \sqrt{(\tau_S - \tau_D)^2 + 4\tilde{g}_S\tilde{g}_D\tau_S\tau_S}\right). \tag{3.2}$$

Here, $\tau_A = C_A/(g_A + g_C)$ for $A = S$ or D.

The plot of the firing rate against either a somatic or a dendritic input current looks rather similar to that of a one-compartment IF neuron. The period diverges logarithmically near the threshold, while for the larger inputs, the f-I relation is

linear. In Appendix A, we show that at the thresholds I_S and I_D, they satisfy

$$\left[I_S + \frac{g_C}{g_C + g_D} I_D\right]_{\text{thresh}} = \left(g_S + g_C \frac{g_D}{g_D + g_C}\right) V_{\text{T}}. \tag{3.3}$$

For large inputs, the firing rate, $R = 1/T$, is to leading order given by

$$R = \frac{1}{C_S(V_{\text{T}} - V_{\text{r}})} \left(I_S + \frac{g_C}{g_C + g_D} I_D\right). \tag{3.4}$$

What does this mean for shunting inhibition? Assuming that the neuron receives no excitatory synaptic input, $g_{eS} = g_{eD} = 0$, and the inhibitory synaptic input is purely shunting at $V_i = 0$, we have $g_S = g_{lS} + g_{iS}$ and $g_D = g_{lD} + g_{iD}$, while the currents, $I_S = I_{0S}$ and $I_D = I_{0D}$, are applied to the respective compartments.

If we apply input only to the soma, $I_D = 0$, the minimal input, $I_{S,\text{thresh}}$, to get the cell to fire is

$$I_{S,\text{thresh}} = \left(g_{lS} + g_{iS} + g_C \frac{g_{lD} + g_{iD}}{g_{lD} + g_{iD} + g_C}\right) V_{\text{T}}. \tag{3.5}$$

For high rates, we have that, to leading order, the firing rate is given by

$$R = \frac{I_S}{C_S(V_{\text{T}} - V_{\text{r}})}. \tag{3.6}$$

Equation (3.5) shows the threshold current increases as the shunting inhibition in the soma or dendrite is increased. Yet, unlike the shunting inhibition in the soma, the increase in the threshold current is due to dendritic shunting saturates. Equation (3.6) shows that for high rates where the relationship between the input current and firing rate is linear, the slope of the f-I curve depends neither on g_{iS} nor on g_{iD}.

In the case where we apply current only to the dendrite, $I_S = 0$, the dendritic threshold current, $I_{D,\text{thresh}}$, above which the neuron starts to fire is given by

$$I_{D,\text{thresh}} = \left[(g_{lS} + g_{iS}) \frac{g_{lD} + g_{iD} + g_C}{g_{lD} + g_{iD}} + g_{lD} + g_{iD}\right] V_{\text{T}}, \tag{3.7}$$

while in the linear part of the f-I curve the slope is given by

$$R = \frac{g_C}{g_{lD} + g_{iD} + g_C} \frac{I_D}{C_S(V_{\text{T}} - V_{\text{r}})}. \tag{3.8}$$

Thus, the threshold for the dendritic current increases linearly with both g_{iS} and g_{iD}, while the slope of the f-I curve depends on g_{iD} but not on g_{iS}.

This is illustrated in Fig. 1. The four panels in this figure show the firing rate, R, plotted against either the current, I_S, injected in the soma (Figs. 1A and 1B), or the injected dendritic current, I_D (Figs. 1C and 1D), for different levels of somatic (Figs. 1A and 1C) or dendritic (Figs. 1B and 1D) shunting inhibition. Table 2 shows the parameters of the IF model used to generate this figure. Increasing shunting inhibition increases the current threshold in all cases, although in the case of somatic

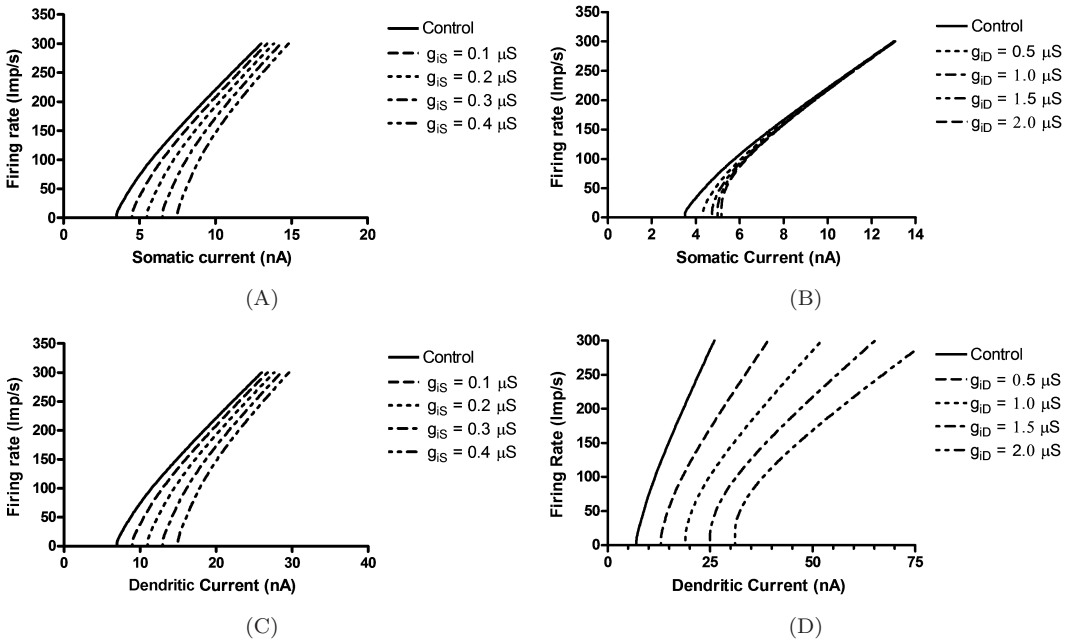

Fig. 1. The effects of somatic and dendritic inhibition on the firing rate gain of the IF model neuron. The term "control" in this and other figures indicates that no inhibitory input is active. In all cases shown in this figure firing was produced by injected currents as specified by the label under each graph's abscissa. Only in the case (D) when firing produced by co-active excitation and inhibition in the dendritic compartment was the firing gain changed.

Table 2. Parameters of the two compartment IF neuron used for Figs. 1 and 2.

Parameter	Value	Parameter	Value
C_S	2 nF	C_D	20 nF
g_{lS}	0.1 μS	g_{lD}	0.5 μS
g_C	0.5 μS	S	25 μVs
V_{T}	10 mV	V_{r}	-10 mV
V_e	50 mV		

input current and dendritic shunting, the effect is small. In the linear range, shunting inhibition at the soma does not change the slope of the f-I curve, but instead shifts the curve along the abscissa (Fig. 1A). If the shunting, inhibition is at the dendrite while the input is at the soma, there is hardly any effect on the linear range of the f-I curve (Fig. 1B). Only in the case where there is dendritic current input and the shunting inhibition is also on the dendrite does the slope of the f-I curve change (Fig. 1D). Thus, shunting inhibition has a subtractive effect if the inhibition is at the soma. If the shunting inhibition is at the dendrite and the current is applied to the soma, the effect is negligible. Only if both target the dendrite, will the shunting inhibition have a divisive effect.

3.2. *Response to constant synaptic inputs*

When the neuron is driven by constant synaptic input, the relationship between the excitatory synaptic conductances g_{eS} and g_{eD}, and the firing period T is still given by Eq. (3.1), even though $g_S = g_{lS} + g_{eS} + g_{iS}$, $g_D = g_{lD} + g_{eD} + g_{iD}$, $V'_S = g_{eS}V_E/(g_S + g_C)$ and $V'_D = g_{eD}V_E/(g_D + g_C)$. The other variables satisfy the same relationship as in the case of the constant injected currents.

Using Eqs. (3.3) and (3.4), one sees that for excitatory synapses at the soma, the conductance required to reach threshold, $g_{eS,\mathrm{thresh}}$, is given by

$$g_{eS,\mathrm{thresh}} = \left(g_{lS} + g_{iS} + g_C \frac{g_{lD} + g_{iD}}{g_{lD} + g_{iD} + g_C}\right) \frac{V_\mathrm{T}}{V_e - V_\mathrm{T}}, \tag{3.9}$$

while for high rates, the gain function becomes linear and the rate satisfies to the leading order

$$R = \frac{V_e}{C_S(V_\mathrm{T} - V_\mathrm{r})} g_{eS}. \tag{3.10}$$

For excitatory synapses projecting to the dendritic compartment, the situation is slightly more complicated. There is an upper limit to the shunting inhibition in the soma, g_{iS}, above which neuron does not fire at all, no matter how large the dendritic excitatory synaptic conductance, g_{eD}. This can be understood by realizing that dendritic synaptic excitation cannot increase the dendritic voltage V_D above the excitatory reversal potential V_e. This puts an upper limit to the amount of current that can flow from the dendrite to the soma. In the sub-threshold regime, the voltage at the soma, V_S, is less than the voltage V which satisfies $V(0) = V_S(0)$ and evolves according to

$$C_S \frac{dV}{dt} = -(g_{lS} + g_{iS})V + g_C(V_e - V), \tag{3.11}$$

and has an equilibrium value, $V_{eq} = \frac{g_C V_e}{g_{lS}+g_{iS}+g_C}$. Thus, if $V_{eq} < V_\mathrm{T}$, or $g_{iS} > g_C(V_e/V_\mathrm{T} - 1) - g_{lS}$, the somatic voltage will never cross the threshold no matter how large g_{eD} is. If g_{iS} is less than this maximum value, Eq. (3.3) gives for the dendritic threshold conductance $g_{eD,\mathrm{thresh}}$

$$g_{eD,\mathrm{thresh}} = \frac{(g_{lS} + g_{iS})(g_{lD} + g_{iD}) + g_C(g_{lS} + g_{iS} + g_{lD} + g_{iD} + g_C)}{g_C(V_e/V_\mathrm{T} - 1) - g_{lS} + g_{iS}}. \tag{3.12}$$

If g_{iS} is not too large, the rate will be high for sufficiently large g_{eD} and we can use Eq. (3.4) to determine the relationship between the firing rate R and the excitatory dendritic conductance

$$R = \frac{g_C}{g_{lD} + g_{eD} + g_{iD} + g_C} \frac{V_e}{C_S(V_\mathrm{T} - V_\mathrm{r})} g_{eD}. \tag{3.13}$$

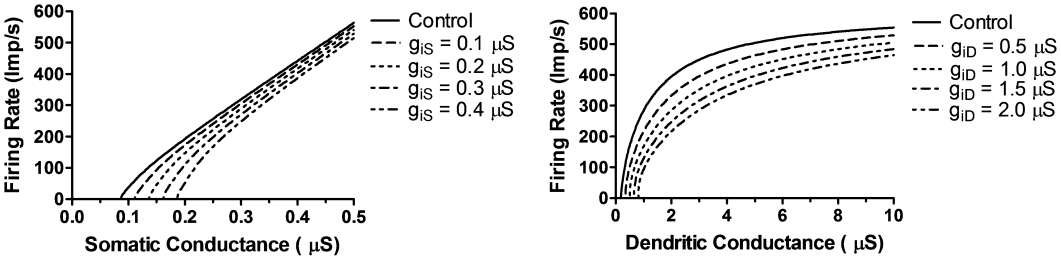

(A) (B)

Fig. 2. The effects of somatic or dendritic inhibitory inputs on the firing rate of the IF model neuron. In these examples firing was produced by either somatic (A) or dendritic (B) excitatory conductance changes. Note how dendritic inhibition (B) reduces the slope (gain) of the relation between firing rate and dendritic excitatory conductance.

Note that firing rate saturates as g_{eD} is increased. The rate does not rise above $R = g_C V_e/(C_S[V_\mathrm{T} - V_\mathrm{r}])$. The explanation for this is while the effective input into the dendrite $I_D = g_{eD}V_e$ increases with the excitatory conductance, so does the effective leak $g_D = g_{lD} + g_{eD} + g_{iD}$. This causes an increased attenuation, so that no matter how strong is the dendritic excitation, the current from dendrite to the soma is bounded.

If the neuron receives both excitatory synaptic input in the soma and in the dendrite, the firing rate for large inputs is given by the sum of Eqs. (3.10) and (3.13). In this case, the firing rate is given by

$$R = \left(g_{eS} + \frac{g_{eD}g_C}{g_{lD} + g_{eD} + g_{iD} + g_C}\right)\frac{V_e}{C_S(V_\mathrm{T} - V_\mathrm{r})}. \tag{3.14}$$

Figure 2 shows the firing rate of the two compartment IF neuron as a function of excitatory synaptic conductance. Figure 2A shows the f-g curve which plots the rate, R against the somatic excitatory conductance, g_{eS}, for different levels of somatic shunting inhibition. The results are similar to those for current injection. The somatic inhibition has a subtractive effect. In Fig. 2B, the firing rate R is plotted against the dendritic excitatory conductance, g_{eD}, for different levels of dendritic inhibition. As expected, the firing rate saturates as g_{eD} is increased. For different levels of dendritic inhibition, the rate asymptotes to the same value but reaches the maximum slower as g_{iD} is increased. Thus, for the same firing rate, the f-g curve is less steep if the dendritic shunt is increased. From Eq. (3.13), we see that for sufficiently high rates, the slope is decreased by a constant fraction. This shows that dendritic shunting inhibition has a divisive effect on dendritic excitatory input. This is shown explicitly in Fig. 3A. In this figure, we plot the slope of the f-g curve (firing gain) against the firing rate. For the same firing rates, the slope of the f-g curve is reduced as g_{iD} is increased.

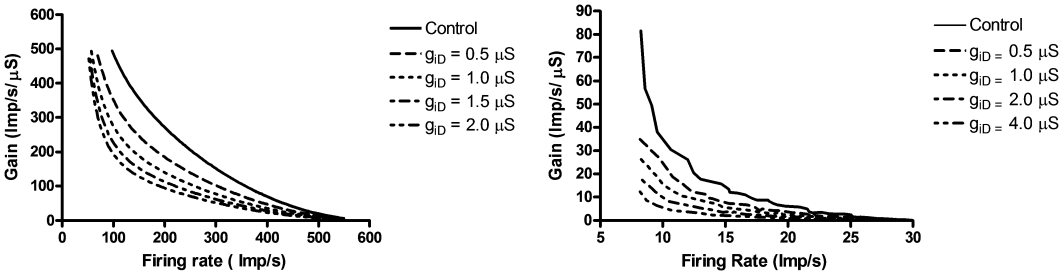

(A) (B)

Fig. 3. The relation between firing rate gain and firing rate produced by dendritic excitatory conductance is shown for the 2-C model IF neuron (A) and the α-motoneuron model (B). Gains were calculated by the central difference formula. Note how the addition of dendritic inhibition (g_{iD}) decreases firing rate gain and that the effect is most pronounced at low and intermediate firing rates. Note that the gain curves for the 2-C IF model neuron converge at very low firing rates because the model does not have a minimum firing rate. By contrast, the firing rate of the α-motoneuron model begins circa 8 Imp/s, consequently the gain curves do not converge at low firing rates.

3.3. *Gain modulation of the conductance based α-motoneuron model*

The relation between firing rate and somatic excitatory conductance for the α-motoneuron model is shown in Fig. 4A. As has been previously reported theoretically [12, 24] and experimentally [9, 41], increasing the inhibitory conductance at the soma results in a translation of the f-g curve to the right along the abscissa, without changing its shape. When the neuron is driven by dendritic excitatory inputs, the firing rate increases nonlinearly and slowly converges to a plateau (Fig. 4B). This is due to the strong and non-linear attenuation of current flowing from the dendritic

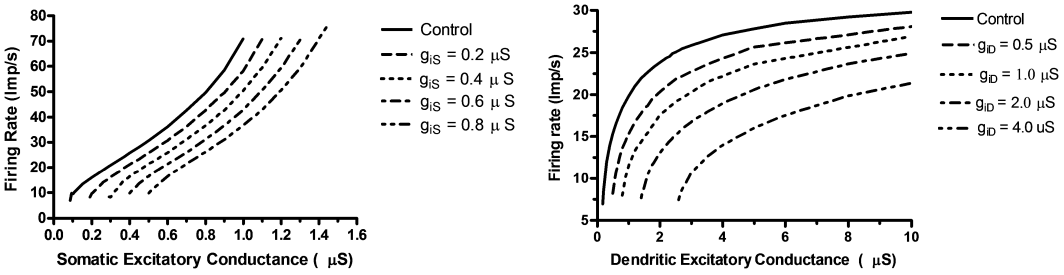

(A) (B)

Fig. 4. The effects of somatic (A) or dendritic (B) inhibitory conductance on the firing rate of the α-motoneuron model. In (A) firing was produced by activating somatic excitatory conductances and in (B) by activating dendritic excitatory conductances. Inhibition at the soma simply translates the relation between firing rate and excitatory conductance to the right. By contrast, dendritic inhibition decreases the firing rate gain when excitation is at the dendrite, as well as also translating the curves to the right. This effect is across the full range of firing rates.

to the somatic compartment, as previously reported [12]. Increasing the dendritic inhibitory conductance not only shifts the curve to the right along the abscissa, but also decreases its slope; the firing gain is thus directly modified (Fig. 4B). This is shown explicitly in Fig. 3B, where firing gain is plotted vs. firing rate. Increasing the dendritic inhibitory conductance from zero to 4μS decreases the gain eightfold at the onset of repetitive firing. By contrast, increasing the dendritic inhibitory conductance translates the curve relating firing rate and somatic excitatory conductance to the right by a small amount, without affecting its shape; while increasing somatic inhibitory conductance translates the curve relating firing rate and dendritic conductance, but not its shape. These effects are similar to those of the IF neuron model.

Equation (3.13) shows that for the IF neuron, the firing rate scales linearly with $g_{eD}/(g_{lD} + g_{eD} + g_{iD} + g_C)$ for sufficiently high rates. In Fig. 5A, the firing rate is plotted against this normalized excitatory dendritic conductance for the IF neuron. Figure 5B shows the same for the α-motoneuron model. For the IF neuron, the plots for different levels of dendritic shunting inhibition perfectly coincide for high rates. For the α-motoneuron, the overlap is not as good but the trend is similar, the curves clearly converge at higher firing rates. The discrepancy is probably due to the limited firing rate range of the α-motoneuron model and the interaction between current flowing from dendrite to soma and the AHP current. It is also interesting to note that the scaling procedure resulted in a quasi-linear relation between normalized dendritic conductance (Fig. 5B) and the firing rate. This contrasts strongly with the non-linear relation between dendritic conductance and the firing rate (Fig. 4B). The observation emphasizes that it is the net current reaching the spike initiation zone at the soma which determines the firing rate. In summary, as predicted by Eq. (3.13), firing rate gain can be modulated by attenuating the current flowing from the dendritic to the somatic compartment. This attenuation occurs naturally

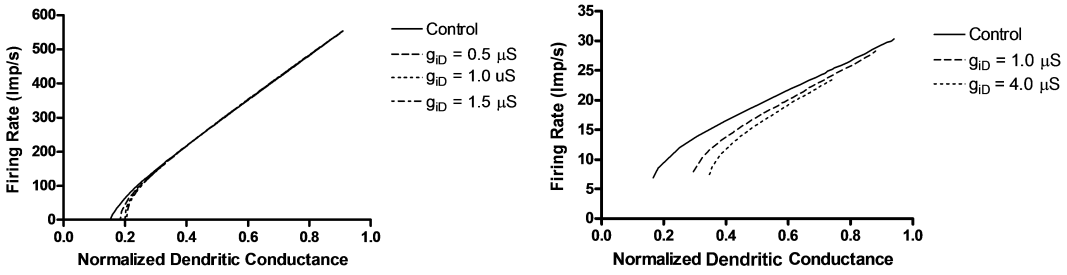

(A) (B)

Fig. 5. The firing rate plotted against the normalized dendritic excitatory conductance for the IF (A) and the α-motoneuron model (B). (A) shows that for the IF model when the dendritic excitatory conductance (g_{eD}) is scaled by $1/(g_{lD} + g_{eD} + g_{iD} + g_C)$ the graphs essentially coincide, except at low rates. Graph (B) shows that the overlap is less good for the α-motoneuron model, but that the trend is similar as for the IF model, the curves tend to converge at higher firing rates. Further details and explanations are given in the text.

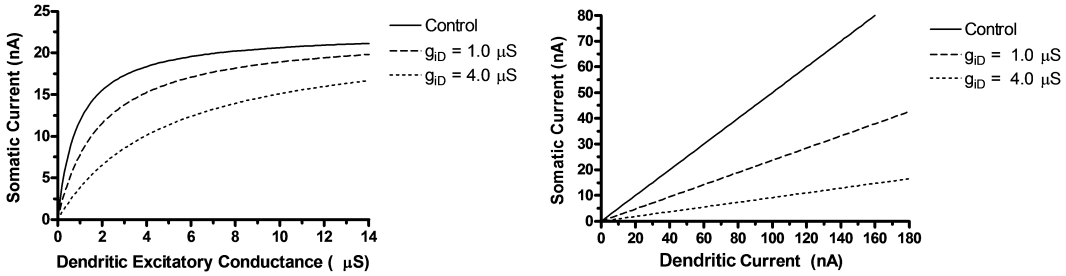

(A) (B)

Fig. 6. Examples of how dendritic current produced by activating synaptic dendritic excitatory conductance (A), or current injected in the dendrite (B), are attenuated at the soma. The somatic and dendritic compartments were voltage clamped. Note that for synaptic currents the relation between dendritic excitatory conductance and current reaching the soma is nonlinear, explaining the nonlinear relation between dendritic excitatory conductance and firing rate. The current reaching the soma is progressively more attenuated as dendritic conductance increases (A). By contrast, the current reaching the soma is attenuated by a constant factor for current injected into the dendrite (B).

and increases progressively as the dendritic excitatory conductance increases on its own (Fig. 6A). Adding inhibition provides a control mechanism by which this current can be further attenuated. As shown in Fig. 6A, increasing the dendritic inhibitory conductance attenuates in a divisive manner, the current flowing from the dendritic to the somatic compartment.

The non-linear relation between firing rate and dendritic excitatory conductance is explained by the progressive attenuation of the current flowing from dendrite to soma (Fig. 6A). By contrast, when current is injected in the dendrite, no change in conductance occurs and the current reaching the soma is linearly related to the injected dendritic current (Fig. 6B). In this case, the slope of the relation is determined by the attenuation factor $g_C/(g_{lD} + g_{eD} + g_{iD} + g_C)$. Clearly, if the dendritic inhibitory conductance is increased, current attenuation also increases (Fig. 6B). The fact that current reaching the soma is linearly related to current injected in the dendrite predicts that the relation between firing rate and current injected in the dendrite will be a monotonically increasing function, as with current injected in the soma. This is in fact the case as shown in Fig. 7A. Predictably, increasing the dendritic inhibitory conductance reduces the slope of this relation and shifts the curve to the right (Fig. 7A). However, when firing is produced by current injected in the soma, increasing the dendritic inhibitory conductance only translates the f-I curve to the right by a small amount (Fig. 7B). The small translation effect is due to the strong attenuation of current, whether excitatory or inhibitory, flowing from dendrite to soma. The lack of effect on the slope of the relation is readily explained by Eq. (3.13). The current produced by activation of the dendritic inhibitory conductance simply adds a constant term to the relation between firing rate and current injected in the soma.

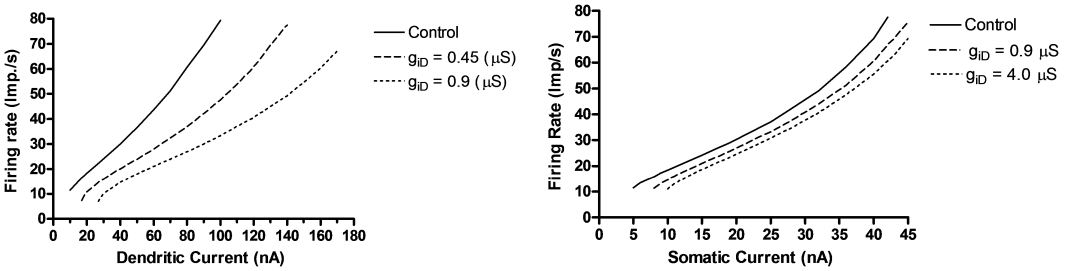

(A) (B)

Fig. 7. Effects of dendritic inhibitory conductance on firing produced by current injected in the dendrite (A) or soma (B). Note the strong effect on gain when firing is produced by dendritic inputs, but not when produced by somatic inputs. Note also that the effects of dendritic inhibition on firing produced by current injected in the soma are weak because of the strong attenuation of current from dendrite to soma.

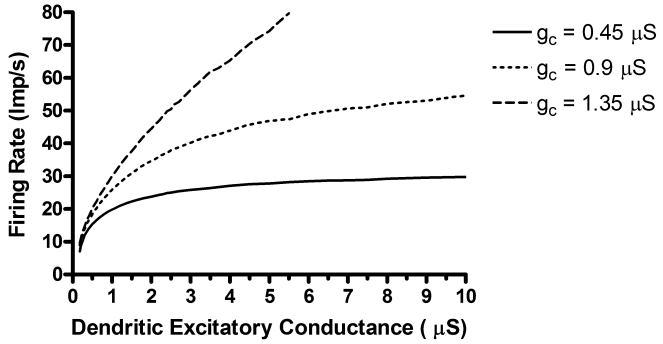

Fig. 8. As the coupling conductance (g_C) between soma and dendrite increases the firing rate gain also increases, because current flowing from dendrite to soma is less attenuated.

The distinction between coupling conductance and dendritic conductance is somewhat artificial, owing to the discrete nature of compartment models of neurons that are in fact continuous structures. Thus, as is clear from Eq. (3.13), changing the coupling conductance will have a direct effect on firing rate gain (Fig. 8). Physiologically, this would be equivalent to increasing inhibition on the proximal dendrites, with the excitatory inputs arriving at the more distal portions.

4. Discussion

The main new finding in this report is that dendritic inhibition leads to a direct change of a neuron's firing rate gain for excitatory inputs that arrive at the dendrite, but not for inputs arriving at the soma. The mechanism can be understood in a straightforward manner and is captured by Eqs. (3.8) and (3.13). The gain change is due to attenuation of current flowing from dendrite to soma, by shunting dendritic inhibition. The gain control mechanism we propose is understandable in

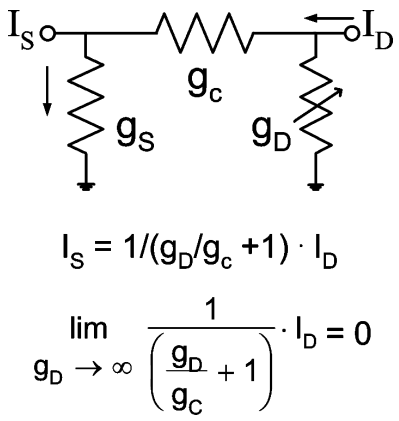

Fig. 9. The π-network composed of three conductances (g_S, g_D, g_C) nicely explains why control of the dendritic conductance (shunting) affects the firing rate gain of neurons. The equation relating the proportion of the dendritic current (I_D) flowing into the soma (I_S) is shown below the π-network. The salient feature of this equation is the attenuation factor, $1/(g_D/g_C + 1)$, which explains why current flowing into the soma from the dendrite is progressively attenuated as the dendritic conductance increases (i.e., in the limit, $I_S \to 0$ as $g_D \to \infty$). The gain of the relation between firing rate and dendritic current will thus depend on the attenuation factor, $1/(g_D/g_C + 1)$.

an intuitive and formally correct manner by considering a simple three conductance π-network neuron model (Fig. 9). The soma and dendrite are represented by single conductances, g_S and g_D respectively, linked by a coupling conductance g_C. In this equivalent representation, the current reaching the soma (I_S) is related to the current coming from the dendrite (I_D) by $I_S = I_D/(g_D/g_S + 1)$. The salient feature of this equation is the attenuation factor $1/(g_D/g_S + 1)$, which explains why current flowing to the soma from the dendrite is progressively attenuated, as the dendritic conductance increases (i.e., in the limit, $I_S \to 0$ as $g_D \to \infty$). The gain of the relation between firing rate and dendritic current will thus depend on the attenuation factor, $1/(g_D/g_S + 1)$. The two compartment models we used, allowed us to obtain analytical expressions relating firing rate to inputs, either injected currents or synaptically activated conductances, and thus determine the factors that can change the firing rate gain. The predictions were verified using a simple conductance-based α-motoneuron model. A noteworthy observation was that dendritic inhibition acts to decrease gain over the full range of firing rates possible with dendritic excitation. The dendritic compartment of the present α-motoneuron model was assumed to be passive, but active conductances such as L-type Ca^{++} channels can be incorporated in the model [7]. In the event, the dendritic inhibitory shunt is likely to have an even more dramatic effect, since dendritic inhibition will suppress activation of the active dendritic currents [31] and reduce gain in the secondary firing range. Something of this sort was in fact observed by Granit *et al.* [19], but they could not appreciate at the time that the effect was likely due to a reduction of the L-type Ca^{++} conductance.

We emphasize that the mechanism we propose does not rely on assumed processes such as noisy excitatory inputs interacting with tonic shunting inhibition [32], or on noisy, balanced, excitatory and inhibitory background activity [15]; neither does it depend on saturation of dendritic voltage interacting with threshold smoothing by noise, as suggested by Prescott and De Koninck [36]. In fact, the conclusion in the latter numerical simulation study that the reported gain changes are the result of dendritic saturation, is incorrect. Indeed, we have shown that shunting inhibition also reduces the gain of the neuron to current injected into the dendrite, and with current injection the dendritic voltage does not saturate. Furthermore, our gain control mechanism does not depend on a non-linear relation between dendritic excitation and somatic depolarization interacting with noisy inputs, as suggested by Prescott and De Koninck [36]. The non-linear relation between dendritic excitation and somatic depolarization explains the non-linear relation between dendritic excitation and firing rate (Fig. 5B), but it is not the basis of a gain control mechanism. Gain control by dendritic shunting inhibition arises naturally from co-active dendritic excitatory and inhibitory inputs. The extent of the mechanism proposed by Chance *et al.* [15], Mitchell and Silver [32] and by us, may be simultaneously operative during neural circuit functions, as well as be mutually reinforcing. It should be noted, however, that the latter mechanisms are somato-centric. They depend on excitation and inhibition at the soma, whereas most neuron inputs are on the dendritic tree and the two types of inputs overlap. For example, 70% of excitatory and 80% of inhibitory inputs are located more than 100 μm away from the soma of motoneurons [8, 10]. Likewise, overlap of excitatory and inhibitory inputs on the dendritic shafts of cortical and hippocampal pyramidal cells have been demonstrated [20, 39]. The gain control mechanism we propose is thus naturally consonant with a prominent feature of neural circuit organization, i.e., the extensive overlap of excitatory and inhibitory synapses on the dendritic tree of neurons. Furthermore, it is clear that with the mechanism proposed here, different levels of shunting inhibition applied to different parts of a neuron's dendritic tree, such as the apical versus basal dendrites of pyramidal neurons, should result in differential gain modulation. The gain may thus be independently controlled at different input ports. This makes for a potentially input-specific control mechanism.

4.1. *Experimental predictions*

Our hypothesis is readily testable in a variety of well described neural circuits. For example, inputs to mammalian α-motoneurons coming from Ia-inhibitory interneurons (Ia-IN) are located closer to the soma, compared with those from Renshaw neurons which are on the proximal dendrites [17]. Consequently, Ia-IN inhibition should have a mainly subtractive effect on f-I curves, consistent with previously published experimental data [19, 23]. By contrast, our hypothesis predicts that motoneuron firing produced by Ia-afferents, 90% of which are on the dendrites, should have a lower gain when co-activated with Renshaw cell inputs. This would correspond to

the model results presented in Fig. 8 where current from dendrite to soma was controlled by the coupling conductance. Experimentally, this may be done by, for example, simultaneously stretching the antagonistic ankle muscles in the decerebrate cat. Our results predict that: (1) the relation between muscle length (input) and motoneuron firing rate will be non-linear, since more than 90% of Ia afferent synapses are distributed across the dendritic tree, and (2) the gain of this relation will not change when Ia-afferent excitation is simultaneous with inhibition coming from the Ia-INs of the antagonistic muscle. However, when Renshaw inhibition is changed in an open-loop manner [13], the firing rate gain should change.

4.2. *Limitations*

We re-emphasize that the main effect of dendritic inhibition on firing rate gain does not depend on a non-linear relation between input and firing rate (e.g., compare Figs. 4B versus 6B). However, different firing profiles, near rheobase, will be somewhat differently affected. For neurons that begin to discharge at a non-zero rate, such as motoneurons, dendritic inhibition will have an obvious effect on gain across the firing range, whereas for neurons that are capable of firing at an arbitrarily low rate, such as pyramidal cells in sensory cortices, the effect of dendritic inhibition will only reduce gain in the approximately linear portion of the f-I curve (i.e., at higher frequencies). However, during dynamic operation of the nervous system, there are presumably random fluctuations of synaptic activity (noise) which smears out the threshold non-linearity [2, 21]. The recent work of Chance *et al.* [15] suggests that this may extend the region across which dendritic shunting inhibition has a divisive effect on firing rate gain.

4.3. *Epilogue*

To what extent modulation of firing rate gain is important in the moment-to-moment operations of the nervous system in its various functions such as attention, sensory processing and motor control remains to be elucidated. To our knowledge, there is no direct evidence that firing rate gain is causal to a class of neural processing operations, rather than simply being a consequence of these operations; i.e., gain modulation does not imply purposeful gain control. Clearly, however, many examples in which gain control may be important have been described. For example, in weak electric fish, there is no mechanism for controlling the sensitivity of the electroreceptor afferents or their synaptic effects. These afferents synapse directly on E-cells of the first sensory relay nucleus. It has been shown that the gain through this nucleus is modified without a significant change of the baseline spontaneous activity of the output E-cells of this nucleus [5, 6], but the mechanism(s) has been elusive [16]. In the motor system, gain control of reflex pathways appear to be important for proper motor performance [27, 37, 40]. More complex gain modulations have been reported in neocortical neurons. For example, the firing rate of posterior parietal

neurons is a function of retinal location. However, the spatial location of the eye scales the relation in a multiplicative manner [3]. Thus, the gain of the response at each retinal locus depends on eye position. The reader should note that the firing rate is a function of retinal locus and eye position, but that these variables may not be related in a simple manner to the currents that drive cell firing. The gain change is thus relative to external variables, but not necessarily relative to the currents that actually drive the firing. It is conceivable that the gain between firing rate and driving current is in fact the same at all eye positions, but that the currents may be a function of eye position leading to an apparent gain change. This example serves to caution against inferring gain changes between variables linked by a complex chain of neural circuits. Because gains are multiplicative, gain may be changed anywhere in the chain, but not necessarily at the recorded neuron. The recent work of Murphy and Miller [33] emphasizes the difference between the firing rate versus stimulus parameter relation, and that of firing rate versus the currents that drive the neuron.

In conclusion, here we have demonstrated a direct and physiologically plausible mechanism by which direct control of firing rate gain may be effected in the CNS. However, this is unlikely to be the sole mechanism. Firing rate gain can also be controlled by actions at the presynaptic terminal [1, 13], by inhibitory feedback which is a function of the neurons firing rate, or by neuromodulator substances that affect intrinsic inward or outward currents [29].

Appendix A. Two-Compartment IF Model

A.1. *Response to constant current inputs*

Between spikes for $0 < t < T$, the voltages V_D and V_S satisfy Eqs. (2.9) and (2.10) with $I_{\text{spike}} = 0$. By dividing both sides of the Eq. (2.9) by $g_D + g_C$ and both sides of Eq. (2.10) by $g_S + g_C$, these equations can be written as

$$\tau_D \frac{dV_D}{dt} = V_D' - V_D + \tilde{g}_S V_S \tag{A.1}$$

and

$$\tau_S \frac{dV_S}{dt} = V_S' - V_S + \tilde{g}_D V_D, \tag{A.2}$$

where $\tau_A = C_A/(g_A + g_C)$ and $V_A' = I_A/(g_A + g_C)$, while $\tilde{g}_S = g_C/(g_D + g_C)$ and $\tilde{g}_D = g_C/(g_S + g_C)$.

Solutions of these equations can be written as

$$V_A(t) = V_{A0} + V_{A+} e^{-\lambda_+ t} + e^{-\lambda_- t} V_{A-} \quad \text{for } A = S, D, \tag{A.3}$$

where $\lambda_\pm$ are the solutions of $(\tau_S\lambda - 1)(\tau_D\lambda - 1) - \tilde{g}_S\tilde{g}_D = 0$,

$$\lambda_\pm = \frac{1}{2\tau_S\tau_D}\left(\tau_S + \tau_D \pm \sqrt{(\tau_S - \tau_D)^2 + 4\tau_S\tau_D\tilde{g}_S\tilde{g}_D}\right). \tag{A.4}$$

Inserting Eq. (A.3) into Eqs. (A.1) and (A.2), one obtains

$$V_{S0} = \frac{V'_S + \tilde{g}_D V'_D}{1 - \tilde{g}_S \tilde{g}_D}, \quad V_{D0} = \frac{V'_D + \tilde{g}_S V'_S}{1 - \tilde{g}_S \tilde{g}_D} \tag{A.5}$$

and

$$V_{D\pm} = \frac{1 - \tau_S \lambda_\pm}{\tilde{g}_D} V_{S\pm}. \tag{A.6}$$

The values of V_{S+} and V_{S-} have to be determined by the relationships between the voltages at times $t = 0$ and $t = T$.

Using $V_D(0) - V_D(T) = g_C S/C_D = \tilde{g}_S S/\tau_D$, we obtain

$$(1 - \tau_S \lambda_+) V_{S+} \left(1 - e^{-\lambda_+ t}\right) + (1 - \tau_S \lambda_-) V_{S-} \left(1 - e^{-\lambda_- t}\right) = \frac{\tilde{g}_S \tilde{g}_D}{\tau_D} S, \tag{A.7}$$

while $V_S(0) - V_S(T) = V_\mathrm{r} - V_\mathrm{T} - \tilde{g}_S \tilde{g}_D S/\tau_S$ yield

$$V_{S+} \left(1 - e^{-\lambda_+ t}\right) + V_{S-} \left(1 - e^{-\lambda_- t}\right) = V_\mathrm{r} - V_\mathrm{T} - \frac{\tilde{g}_S \tilde{g}_D}{\tau_S} S. \tag{A.8}$$

Solving these two equations for $V_{S\pm}$, we obtain

$$V_{S\pm} = \frac{(1 - \tau_S \lambda_\mp)(V_\mathrm{T} - V_\mathrm{r}) + \lambda_\pm \tilde{g}_S \tilde{g}_D S}{\tau_S (\lambda \mp -\lambda \pm)(1 - e^{-\lambda_\pm t})}. \tag{A.9}$$

Finally, to get the relationship between I_S, I_D and T, we need to impose the constraint that at time $t = T$, the somatic voltage is at the threshold, $V_S(T) = V_\mathrm{T}$. This yields the input-output relationship

$$\begin{aligned} &\tau_s(\lambda_+ - \lambda_-) \frac{V'_S + \tilde{g}_D V'_D}{1 - \tilde{g}_S \tilde{g}_D} \\ &\quad = \tilde{g}_S \tilde{g}_D S \left(\frac{\lambda_+ e^{-\lambda_+ T}}{1 - e^{-\lambda_+ T}} - \frac{\lambda_- e^{-\lambda_- T}}{1 - e^{-\lambda_- T}} \right) + V_\mathrm{T} \left(\frac{1 - \tau_S \lambda_-}{1 - e^{-\lambda_+ T}} - \frac{1 - \tau_S \lambda_+}{1 - e^{-\lambda_- T}} \right) \\ &\qquad + V_\mathrm{r} \left(\frac{(1 - \tau_S \lambda_+)^{-\lambda_- T}}{1 - e^{-\lambda_- T}} - \frac{(1 - \tau_S \lambda_-) e^{-\lambda_+ T}}{1 - e^{-\lambda_+ T}} \right). \end{aligned} \tag{A.10}$$

A.2. *The current threshold*

If the input is below threshold, the neuron does not emit spikes. The threshold input can be found by taking the limit $T \to \infty$ in Eq. (A.10), or alternatively, by setting $V_{S0} = V_\mathrm{T}$. This yields for the threshold

$$\frac{V'_S + \tilde{g}_D V'_D}{1 - \tilde{g}_S \tilde{g}_D} = V_\mathrm{T}, \tag{A.11}$$

which can be written as

$$\left[I_S + \frac{g_C}{g_D + g_C} I_D\right] = \left(g_S + g_C \frac{g_D}{g_D + g_C}\right) V_{\mathrm{T}} \tag{A.12}$$

using the definitions of V'_S, V'_D, $\tilde{g}_S$ and $\tilde{g}_D$.

A.3. *High rate approximation*

If the input is large, and the firing rate is high, we can approximate Eq. (A.10). For high rate $T \ll 1$, $e^{-\lambda_\pm T} \approx 1 - \lambda_\pm T$. Inserting this in Eq. (A.10), we obtain

$$\tau_S \frac{V'_S + \tilde{g}_D V'_D}{1 - \tilde{g}_S \tilde{g}_D} = \frac{V_{\mathrm{T}} - V_{\mathrm{r}}}{\lambda_+ \lambda_- T}[(\lambda_+ + \lambda_-)\tau_S - 1]. \tag{A.13}$$

Using

$$\lambda_+ \lambda_- = \frac{1 - \tilde{g}_S \tilde{g}_D}{\tau_S \tau_D} \quad \text{and} \quad \lambda_+ + \lambda_- = \frac{1}{\tau_S} + \frac{1}{\tau_D}, \tag{A.14}$$

this can be simplified to

$$V'_S + \tilde{g}_D V'_D = \frac{(V_{\mathrm{T}} - V_{\mathrm{r}})\tau_S}{T}. \tag{A.15}$$

Therefore, the firing rate $R = 1/T$ is, to leading order, given by

$$R = \frac{1}{C_M(V_{\mathrm{T}} - V_{\mathrm{r}})} \left(I_S + \frac{g_C}{g_D + g_C} I_D\right). \tag{A.16}$$

Acknowledgments

C. Capaday was supported by the Natural Sciences and Engineering Research Council of Canada (NSERC), and in part by the Canadian Institutes of Health Research (CIHR). C. van Vreeswijk was supported by HFSP grant RGY0014/2002. We thank Drs. Nicolas Brunel, Claude Meunier and Daniel Zytnicki for their comments and suggestions on a draft of this manuscript.

References

[1] Abbott LF, Varela JA, Sen K, Nelson SB, Synaptic depression and cortical gain control, *Science* **275**:220–224, 1997.

[2] Amit DJ, Brunel N, Model of global spontaneous activity and local structured activity during delay periods in the cerebral cortex, *Cereb Cortex* **7**:237–252, 1997.

[3] Andersen RA, Zipser D, The role of the posterior parietal cortex in coordinate transformations for visual-motor integration, *Can J Physiol Pharmacol* **66**:488–501, 1988.

[4] Barrett EF, Barrett JN, Crill WE, Voltage-sensitive outward currents in cat motoneurones, *J Physiol* **304**:251–276, 1980.

[5] Bastian J, Gain control in the electrosensory system mediated by descending inputs to the electrosensory lateral line lobe, *J Neurosci* **6**:553–562, 1986.

[6] Bastian J, Gain control in the electrosensory system: A role for the descending projections to the electrosensory lateral line lobe, *J Comp Physiol A* **158**:505–515, 1986.
[7] Booth V, Rinzel J, Kiehn O, Compartmental model of vertebrate motoneurons for Ca^{2+}-dependent spiking and plateau potentials under pharmacological treatment, *J Neurophysiol* **78**:3371–3385, 1997.
[8] Brännström T, Quantitative synaptology of functionally different types of cat medial gastrocnemius alpha-motoneurons, *J Comp Neurol* **330**:439–454, 1999.
[9] Brizzi L, Meunier C, Zytnicki D, Donnet M, Hansel D, D'Incamps BL, Van Vreeswijk C, How shunting inhibition affects the discharge of lumbar motoneurones: A dynamic clamp study in anaesthetized cats, *J Physiol* **558**:671–683, 2004.
[10] Burke RE, Spinal cord: Ventral horn, in Shepherd GM (ed.), *The Synaptic Organization of the Brain*, Oxford University Press, Oxford, 1998.
[11] Capaday C, The special nature of human walking and its neural control, *Trends Neurosci* **25**:370–376, 2002.
[12] Capaday C, A re-examination of the possibility of controlling the firing rate gain of neurons by balancing excitatory and inhibitory conductances, *Exp Brain Res* **143**: 67–77, 2002.
[13] Capaday C, Stein RB, A method for simulating the reflex output of a motoneuron pool, *J Neurosci Meth* **21**:91–104, 1987.
[14] Capaday C, Stein RB, The effects of postsynaptic inhibition on the monosynaptic reflex of the cat at different levels of motoneuron pool activity, *Exp Brain Res* **77**: 577–584, 1989.
[15] Chance FS, Abbott LF, Reyes AD, Gain modulation from background synaptic input, *Neuron* **35**:773–782, 2002.
[16] Doiron B, Longtin A, Berman N, Maler L, Subtractive and divisive inhibition: Effect of voltage-dependent inhibitory conductances and noise, *Neural Comput* **13**: 227–248, 2001.
[17] Fyffe RE, Spatial distribution of recurrent inhibitory synapses on spinal motoneurons in the cat, *J Neurophysiol* **65**:1134–1149, 1991.
[18] Granit R, *Mechanisms Regulating the Discharge of Motoneurons*, Charles C. Thomas Publisher, Springfield, 1972.
[19] Granit R, Kernell D, Lamarre Y, Synaptic stimulation superimposed on motoneurones firing in the "secondary range" to injected current, *J Physiol* **187**:401–415, 1966.
[20] Halasy K, Cobb SR, Buhl EH, Nyiri G, Somogyi P, Sites of synaptic junctions established by a GABAergic basket cell on an interneuron in the CA1 area of the rat hippocampus, *Neurobiol* **4**:269–270, 1996.
[21] Hansel D, van Vreeswijk C, How noise contributes to contrast invariance of orientation tuning in cat visual cortex, *J Neurosci* **22**:5118–5128, 2002.
[22] Heckman CJ, Computer simulations of the effects of different synaptic input systems on the steady-state input-output structure of the motoneuron pool, *J Neurophysiol* **71**:1727–1739, 1994.
[23] Henneman E, Mendell LM, Functional organization of motoneuron pool and its inputs, in Brooks VB (ed.), *The Nervous System*, American Physiological Society, Bethesda, pp. 423–507, 1981.
[24] Holt GR, Koch C, Shunting inhibition does not have a divisive effect on firing rates, *Neural Comput* **9**:1001–1013, 1997.

[25] Lapique L, Recherches quantitatives sur l'excitation electrique des nerfs traitée comme une polarization, *J Physiol Pathol Gen* **9**:620–635, 1907.

[26] Llinas RR, Walton KD, Cerebellum, in Sheperd GM (ed.), *The Synaptic Organization of the Brain*, Oxford University Press, Oxford, pp. 255–288, 1998.

[27] Lisberger SG, Learning and memory in the vestibuloocular reflex, in Bloedel JR, Ebner TJ, Wise SP (eds.), *The Acquisition of Motor Behavior in Vertebrates*, MIT Press, Cambridge, pp. 7–28, 1996.

[28] Matthews PB, The effect of firing on the excitability of a model motoneurone and its implications for cortical stimulation, *J Physiol-London* **518**:867–882, 1999.

[29] McCormick DA, Membrane properties and Neurotransmitter actions, in Shepherd GM (ed.), *The Synaptic Organization of the Brain*, Oxford University Press, Oxford, pp. 32–66, 1998.

[30] Meunier C, Borejsza K, How membrane properties shape the discharge of motoneurons: A detailed analytical study, *Neural Comput* **17**:2383–2420, 2005.

[31] Miles R, Tóth K, Gulyás AI, Hájos N, Freund FT, Difference between somatic and dendritic inhibition in the hippocampus, *Neuron* **16**:815–823, 1996.

[32] Mitchell SJ, Silver RA, Shunting inhibition modulates neuronal gain during synaptic excitation, *Neuron* **38**:433–445, 2003.

[33] Murphy BK, Miller KD, Multiplicative gain changes are induced by excitation or inhibition alone, *J Neurosci* **23**:10040–10051, 2003.

[34] Powers RK, A variable-threshold motoneuron model that incorporates time- and voltage-dependent potassium and calcium conductances, *J Neurophysiol* **70**: 246–262, 1993.

[35] Powers RK, Binder MD, Input-output functions of mammalian motoneurons, *Rev Physiol Biochem Pharmacol* **143**:137–263, 2001.

[36] Prescott SA, De Koninck Y, Gain control of firing rate by shunting inhibition: Roles of synaptic noise and dendritic saturation, *P Natl Acad Sci USA* **100**:2076–2081, 2003.

[37] Prochazka A, Sensorimotor gain control: A basic strategy of motor systems? *Prog Neurobiol* **33**:281–307, 1989.

[38] Salinas E, Abbott LF, A model of multiplicative neural responses in parietal cortex, *P Natl Acad Sci USA* **93**:11956–11961, 1996.

[39] Somogyi P, Tamas G, Lujan R, Buhl EH, Salient features of synaptic organisation in the cerebral cortex, *Brain Res Rev* **26**:113–135, 1998.

[40] Stein RB, Capaday C, The modulation of human reflexes during functional motor tasks, *Trends Neurosci* **11**:328–332, 1988.

[41] Ulrich D, Differential arithmetic of shunting inhibition for voltage and spike rate in neocortical pyramidal cells, *Eur J Neurosci* **18**:2159–2165, 2003.